Turkish Journal of Engineering
https://dergipark.org.tr/en/pub/tuje
e-ISSN 2587-1366

Determination of the critical drop height and critical flow velocity of aluminum alloy (AL-91% Mg-8% Fe-0.4% Zn-0.2%) in gravity sand casting

Francis Inegbedion [*1], **James Chinedu Orji** [1]

[1]*University of Benin, Department of Production Engineering, Nigeria*

Keywords
Critical drop height
Critical velocity
Gravity sand casting
Finite element method
Sprue

Research Article
DOI: 10.31127/tuje.1077467

Received: 22.02.2022
Accepted: 20.04.2022
Published: 26.04.2022

Abstract

Casting is a manufacturing process in which molten metal is poured through the gating system to fill the mould cavity where it solidifies. Variations in casting parameters by different researchers have led to significant variations in casting guidelines, which have forced Foundry Engineers to carry out a number of trial-and-error runs to create guidelines based on their own experience. These variations in guidelines have led to defects occurring in casting during the mould filling process. This work aimed at determining the critical drop height and critical flow velocity of a certain molten aluminum alloy as it flow down the mould sprue in gravity sand casting. The continuity equation was used to describe the velocity distribution of the aluminum alloy as it flows down the sprue. The mathematical tool used in this research is the finite element method. It involves the discretization of the domain of interest into smaller finite elements. The weak form of the governing equation was obtained and integrated over the domain of interest. The results obtained, established the critical flow velocity of aluminum alloy, down the sprue, as 2.565×10^3 mm/s and the critical drop height as 377mm. Results obtained were compared with literature and were also used to produce various casts, it was observed that casts produced, using sprue height below the critical drop height obtained prevented casting defects, while at sprue height above the critical drop height, the danger of casting defects could not be avoided.

1. Introduction

Casting is a manufacturing process in which liquid metal is usually poured into a mould cavity of the desired shape, and then allowed to solidify. The solidified part is known as casting, which is ejected or broken out of the mould to complete the process. There are two main consecutive stages: filling process and solidification process. In filling process, gating system, comprising the pouring cup, runner, sprue, sprue well and in-gate, is designed to guide molten metal into the mould cavity for filling. The riser system is used to compensate for shrinkage caused by casting solidification [1].

Mould filling is a very important step in determining the quality of a casting. The fluid flow phenomenon during the mould filling is closely related to the casting quality, surface finish and macro segregation of the cast part and mould erosion. Dimensional accuracy of casting is affected by the flow in the mould cavity. Modeling of the mould filling is a very complex process, since many physical phenomena, such as free surface flow, turbulence, surface tension and combination of fluid flow with heat transfer, should be considered. In order to take all these parameters into account, the computing technique tends to be complicated [2].

Pouring turbulence during mould filling is detrimental to the quality of sand castings. The formation of various castings defects could be directly related to the fluid flow phenomena involved in the stage of mould filling. For instance, vigorous steam could cause mould erosion; highly turbulent flows could result in air and inclusions entrapments; and relatively slower filling might generate cold shut [2]. Furthermore, porosity, a common defect in casting also could result from improper design of gating system [3].

The objective of a gating system is to get enough metal into the mould cavity before the metal starts to solidify, minimize turbulence to avoid trapping gases into the mould and establish the best possible temperature gradient in the solidifying casting so that

* **Corresponding Author**

*(francis.inegbedion@uniben.edu) ORCID ID 0000-0002-2142-8079
(jamesorji9396@gmail.com) ORCID ID 0000-0002-6098-6663

Cite this article

Inegbedion, F., & Orji, J. C. (2023). Determination of the critical drop height and critical flow velocity of aluminum alloy (AL-91% Mg-8% Fe-0.4% Zn-0.2%) in gravity sand casting. Turkish Journal of Engineering, 7(2), 149-156

the shrinkage occurs in the gating system not in the cast [4]. For proper functioning of the gating system, the rate at which molten metal is poured to fill the mould cavity must be controlled [5].

These problems not only lead to a long casting development cycle, but also a low reliability of casting design due to variations of individual knowledge and experience. Getting the liquid metal out of the crucible into the mould is a critical step in the casting process. Most casting scrap arises during these few seconds of mould filling. Therefore, the authors seek to streamline the several casting design guidelines by establishing the critical flow velocity and drop height of molten aluminum alloy as it flows down the sprue during gravity sand casting process, having a top riser opened to atmospheric pressure.

2. Method

2.1. Mathematical model employed

The continuity equation of a controlled volume and the finite element method were the models used in analyzing the critical flow velocity and critical drop height of the aluminum alloy.

2.1.1 Analysis of molten metal flow in the mould sprue in gravity sand casting

The governing equations of molten metal flow in gravity sand casting and the finite element method were used in this analysis.

2.1.2 Governing equations

The governing equations of molten metal flow in casting mould cavity are governed by the continuity equations in cylindrical axisymmetric coordinate as shown in Equation (1) [6–10].

$$\frac{\partial P}{\partial t}+\frac{1}{r}\frac{\partial}{\partial r}\left(ru_r\right)+\frac{\partial u_z}{\partial z}=0 \tag{1}$$

At steady state $\frac{\partial}{\partial z}=0$ and Equation (1) becomes

$$\frac{1}{r}\frac{\partial}{\partial r}\left(ru_r\right)+\frac{\partial u_z}{\partial z}=0 \tag{2}$$

The solutions to Equation (2) can only be obtained by applying the appropriate initial and boundary conditions. The initial conditions for pressure and temperature fields are given by Equation (3) [4,6].

$$p(z,t_0)=p_0(z), \qquad T(r,z,t_0)=T_0(r,z) \tag{3}$$

The boundary conditions specified in the considered problem are as indicated in Equations (4) to (7), [5,11–15].

At the inlet gate:

$$u_n=u_{in} \qquad u_t=0 \qquad \text{or} \qquad p=p_{in} \tag{4}$$

At the mould wall:

$$u_r=u_z=0, \qquad \frac{\partial p}{\partial n}=0 \tag{5}$$

At the flow front:

$$p=0 \tag{6}$$

At the cavity center line:

$$\frac{\partial p}{\partial n}=0 \qquad \frac{\partial u_t}{\partial r}=0 \qquad u_r=0 \qquad u_z=u \tag{7}$$

The solutions to Equations (2) were obtained using the finite element method in the weighted residuals formulation [16–18].

2.2. Finite element solution of molten metal flow in the mould sprue

The velocity distribution over the domain of interest is discretized into finite element having M nodes, using suitable interpolation models for $u^{(e)}$ in element e as:

$$u_{(r,z)}=\sum_{i=1}^{m} w(r,z)u=[w]\{u\} \tag{8}$$

and we developed the velocity distribution for Equation (2) using the finite element method, seeking an approximate solution over each finite element. The weighted residual and the weighted integral of Equation (2) are Equations (9) and (10) respectively.

$$w_{(r,z)}\left[\frac{1}{r}\frac{\partial u_r}{\partial r}+\frac{\partial u_z}{\partial z}\right]=0 \tag{9}$$

$$\int_{\Omega_e} w_{(r,z)}\left[\frac{1}{r}\frac{\partial u_r}{\partial r}+\frac{\partial u_z}{\partial z}\right]drdz=0 \tag{10}$$

We integrated Equation (10) by parts (Equation (11)), to obtain the weak form of Equations (2).

$$-\int_{\Omega_e}\left(u_r\frac{1}{r}\frac{\partial w}{\partial r}+u_z\frac{\partial w}{\partial z}\right)\partial r\partial z+w\left(u_z+u_r\frac{1}{r}\right)\Big|_{\Omega_e}=0 \tag{11}$$

The finite element model (Equation 13) was developed by substituting Equations (8) and (10) into Equation (11) to obtain Equation (12).

$$\int_{\Omega_e} w\left(\frac{1}{r}\frac{\partial w}{\partial r}+\frac{\partial w}{\partial z}\right)\partial r\partial z\{u\}=w\left(u_z+u_r\frac{1}{r}\right)\Big|_{\Omega_e} \tag{12}$$

In matrix form Equation (12) becomes

$$\left|K_{ij}{}^{e}\right|\{u\}=\left\{Q_{ij}{}^{e}\right\} \tag{13}$$

Where $\left|K_{ij}^{\ e}\right|$ the M x M matrix is

$$\left|K_{ij}^{\ e}\right| = \int_{\Omega_e} w\left(\frac{1}{r}\frac{\partial w}{\partial r} + \frac{\partial w}{\partial z}\right)\partial r \partial z \tag{14}$$

and $\{Q_{ij}^{e}\}$ represented by M x 1 column matrix is

$$\left\{Q_{ij}^{\ e}\right\} = w\left(u_z + u_r\frac{1}{r}\right)\Big|_{\Omega_e} \tag{15}$$

To simplify the $\left|K_{ij}^{\ e}\right|$ and $\left\{Q_{ij}^{\ e}\right\}$, we used a linear rectangular element (Figure 1) to develop our interpolation model

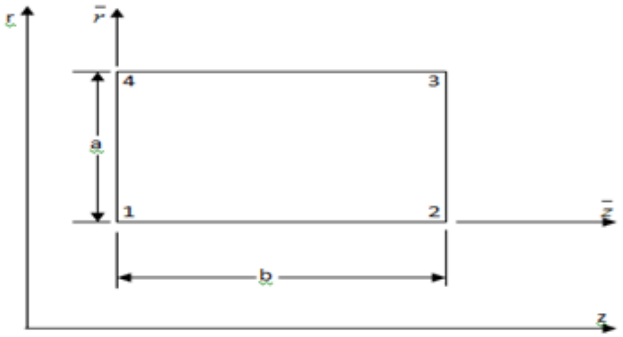

Figure 1. Geometry of the element

Firstly, we obtained the interpolation model for the K^e matrices by considering an approximation of the form:

$$w(r,z) = c_1 + c_2 r + c_3 z + c_4 rz \tag{16}$$

and used a linear rectangular element sides *a* and *b* (with *r* = *a* and *b* = *z*) (Figure 1).

$$w(r,z) = c_1 + c_2 a + c_3 b + c_4 ab \tag{17}$$

and require

$$\begin{aligned} w_1 &= w(0,0) = c_1 \\ w_2 &= w(a,0) = c_1 + c_2 a \\ w_3 &= w(a,b) = c_1 + c_2 a + c_3 b + c_4 ab \\ w_4 &= w(0,b) = c_1 + c_3 b \end{aligned} \tag{18}$$

The solutions for $c_i\,(i = 1,\ldots,4)$, in Equations (18) are

$$c_1 = w_1 \qquad c_2 = \frac{w_2 - c_1}{a} = \frac{w_2 - w_1}{a} \tag{19}$$

$$c_3 = \frac{w_4 - c_1}{b} = \frac{w_4 - w_1}{b}$$

$$c_4 = \frac{w_3 - c_1 - c_2 a - c_3 b}{ab} = \frac{w_3 - w_1 - w_2 - w_1 - w_4 - w_1}{ab} = \frac{w_3 - w_4 + w_1 - w_2}{ab}$$

We substituted Equation (19) into Equation (17) and noting that *a* = *r* and *b* = *z* to obtain Equation (20)

$$w(r,z) = \left(1-\frac{r}{a}\right)\left(1-\frac{z}{b}\right)w_1 + \frac{r}{a}\left(1-\frac{z}{b}\right)w_2 + \frac{rz}{ab}w_3 + \frac{z}{b}\left(1-\frac{r}{a}\right)w_4 \tag{20}$$

Equation (20) becomes Equation (21)

$$w(r,z) = \theta_1 w_1 + \theta_2 w_2 + \theta_3 w_3 + \theta_4 w_4 \tag{21}$$

Where

$$\begin{aligned} \theta_1 &= \left(1-\frac{r}{a}\right)\left(1-\frac{z}{b}\right) & \theta_2 &= \frac{r}{a}\left(1-\frac{z}{b}\right) \\ \theta_3 &= \frac{rz}{ab} & \theta_4 &= \frac{z}{b}\left(1-\frac{r}{a}\right) \end{aligned} \tag{22}$$

We differentiated Equation (22) with respect to *r* and *z* to obtain Equation (23).

$$\begin{aligned} \frac{d\theta_1}{dr} &= \left(-\frac{1}{a}\right)\left(1-\frac{z}{b}\right) = \left(\frac{-1}{a} + \frac{z}{ab}\right) \\ \frac{d\theta_1}{dz} &= \left(-\frac{1}{b}\right)\left(1-\frac{r}{a}\right) = \left(\frac{-1}{b} + \frac{r}{ab}\right) \\ \frac{d\theta_2}{dr} &= \frac{1}{a}\left(1-\frac{z}{b}\right) = \frac{1}{a} - \frac{z}{ab} \\ \frac{d\theta_2}{dy} &= -\frac{r}{ab} \\ \frac{d\theta_3}{dr} &= \frac{z}{ab} \\ \frac{d\theta_3}{dz} &= \frac{r}{ab} \\ \frac{d\theta_4}{dr} &= -\frac{z}{ab} \\ \frac{d\theta_4}{dz} &= \frac{1}{b}\left(1-\frac{r}{a}\right) = \frac{1}{b} - \frac{r}{ab} \end{aligned} \tag{23}$$

To derive the respective $\left|K_{ij}^{\ e}\right|$ values we used a four linear rectangular element (Figure 2) to obtain Equation (24).

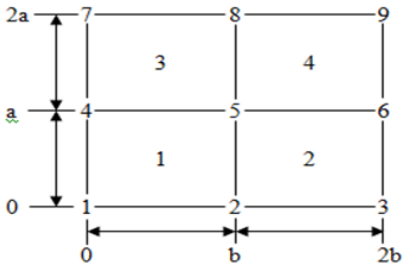

Figure 2. Four Linear Rectangular Elements

$$K_{11}^{1}=\int_0^b\int_0^a\left[\left(\left(-\frac{1}{a}\right)\left(1-\frac{z}{b}\right)\right)^2+\left(\left(-\frac{1}{b}\right)\left(1-\frac{r}{a}\right)\right)^2\right]drdz=\frac{a}{3b}+\frac{b}{3a} \tag{24a}$$

$$K_{12}^{1}=\int_0^b\int_0^a\left[\left(\frac{-1}{a}+\frac{z}{ab}\right)^2+\left(\frac{-1}{b}+\frac{r}{ab}\right)\left(-\frac{r}{ab}\right)\right]drdz=\frac{a}{6b}+\frac{b}{3a} \tag{24b}$$

$$K_{13}^{1}=\int_0^b\int_0^a\left[\left(\frac{-1}{a}+\frac{z}{ab}\right)\left(\frac{z}{ab}\right)+\left(\frac{-1}{b}+\frac{r}{ab}\right)\left(\frac{r}{ab}\right)\right]drdz=\frac{-a}{6b}-\frac{b}{6a} \tag{24c}$$

$$K_{14}^{1}=\int_0^b\int_0^a\left[\left(\frac{-1}{a}+\frac{z}{ab}\right)\left(\frac{-z}{ab}\right)+\left(\frac{-1}{b}+\frac{r}{ab}\right)\left(\frac{1}{b}-\frac{r}{ab}\right)\right]drdz=\frac{a}{3b}+\frac{b}{6a} \tag{24d}$$

$$K_{21}^{1}=K_{12}^{1}=\frac{a}{6b}+\frac{b}{3a} \tag{24e}$$

$$K_{22}^{1}=\int_0^b\int_0^a\left[\left(\frac{1}{a}-\frac{z}{ab}\right)^2+\left(-\frac{r}{ab}\right)^2\right]drdz=\frac{a}{3b}+\frac{b}{3a} \tag{24f}$$

$$K_{23}^{1}=\int_0^b\int_0^a\left[\left(\frac{1}{a}-\frac{z}{ab}\right)\left(\frac{z}{ab}\right)+\left(\frac{-r}{ab}\right)\left(\frac{r}{ab}\right)\right]drdz=\frac{b}{6a}-\frac{a}{3b} \tag{24g}$$

$$K_{24}^{1}=\int_0^b\int_0^a\left[\left(\frac{1}{a}-\frac{z}{ab}\right)\left(\frac{-z}{ab}\right)+\left(\frac{-r}{ab}\right)\left(\frac{1}{b}-\frac{r}{ab}\right)\right]drdz=\frac{b}{6a}-\frac{a}{6b} \tag{24h}$$

$$K_{31}^{1}=K_{13}^{1}=\frac{-a}{6b}-\frac{b}{6a} \qquad K_{32}^{1}=K_{23}^{1}=\frac{b}{6a}-\frac{a}{3b} \tag{24i}$$

$$K_{33}^{1}=\int_0^b\int_0^a\left[\left(\frac{z}{ab}\right)^2+\left(\frac{r}{ab}\right)^2\right]drdz=\frac{a}{3b}+\frac{b}{3a} \tag{24j}$$

$$K_{34}^{1}=\int_0^b\int_0^a\left[\left(\frac{z}{ab}\right)\left(\frac{-z}{ab}\right)+\left(\frac{r}{ab}\right)\left(\frac{1}{b}-\frac{r}{ab}\right)\right]drdz=\frac{a}{6b}-\frac{b}{3a} \tag{24k}$$

$$K_{41}^{1}=K_{14}^{1}=\frac{a}{3b}+\frac{b}{6a} \qquad K_{42}^{1}=K_{24}^{1}=\frac{b}{6a}-\frac{a}{6b} \qquad K_{43}^{1}=K_{34}^{1}=\frac{a}{6b}-\frac{b}{3a} \tag{24l}$$

$$K_{44}^{1}=\int_0^b\int_0^a\left[\left(\frac{-z}{ab}\right)^2+\left(\frac{1}{b}-\frac{r}{ab}\right)^2\right]drdz=\frac{a}{3b}+\frac{b}{3a} \tag{24m}$$

The $\left|K_{ij}^{e}\right|$ matrix is therefore Equations (25) and (26)

$$K=\begin{bmatrix} \frac{a}{3b}+\frac{b}{3a} & \frac{a}{6b}+\frac{b}{3a} & \frac{-a}{6b}-\frac{b}{6a} & \frac{a}{3b}+\frac{b}{6a} \\ \frac{a}{6b}+\frac{b}{3a} & \frac{a}{3b}+\frac{b}{3a} & \frac{b}{6a}-\frac{a}{3b} & \frac{b}{6a}-\frac{a}{6b} \\ \frac{-a}{6b}-\frac{b}{6a} & \frac{b}{6a}-\frac{a}{3b} & \frac{a}{3b}+\frac{b}{3a} & \frac{a}{6b}-\frac{b}{3a} \\ \frac{a}{3b}+\frac{b}{6a} & \frac{b}{6a}-\frac{a}{6b} & \frac{a}{6b}-\frac{b}{3a} & \frac{a}{3b}+\frac{b}{3a} \end{bmatrix} \tag{25}$$

$$K=\frac{b}{6a}\begin{bmatrix} 2 & -2 & -1 & 1 \\ -2 & 2 & 1 & -1 \\ -1 & - & 2 & -2 \\ 1 & -1 & -2 & 2 \end{bmatrix}+\frac{a}{6b}\begin{bmatrix} 2 & 1 & -1 & -2 \\ 1 & 2 & -2 & -1 \\ -1 & -2 & 2 & 1 \\ -2 & -1 & 1 & 2 \end{bmatrix} \tag{26}$$

If *a = 4* and *b = 1* Equation (26) becomes

$$K = \begin{bmatrix} 1.4166 & 0.5834 & -0.7084 & -1.2916 \\ 0.5834 & 1.4166 & -1.2916 & -0.7084 \\ -0.7084 & -1.2916 & 1.4166 & 0.5834 \\ -1.2916 & -0.7084 & 0.5834 & 1.4166 \end{bmatrix} \tag{27}$$

Let, $K^1 = K^2 = K^3 = K^4$,therefore

$$K_{ij}{}^{e} = K^1 + K^2 + K^3 + K^4 \tag{28}$$

$$K_{ij}{}^{e} = \left[\begin{bmatrix} 1.4166 & 0.5834 & -0.7084 & -1.2916 \\ 0.5834 & 1.4166 & -1.2916 & -0.7084 \\ -0.7084 & -1.2916 & 1.4166 & 0.5834 \\ -1.2916 & -0.7084 & 0.5834 & 1.4166 \end{bmatrix} + \begin{bmatrix} 1.4166 & 0.5834 & -0.7084 & -1.2916 \\ 0.5834 & 1.4166 & -1.2916 & -0.7084 \\ -0.7084 & -1.2916 & 1.4166 & 0.5834 \\ -1.2916 & -0.7084 & 0.5834 & 1.4166 \end{bmatrix} + \right. \\ \left. \begin{bmatrix} 1.4166 & 0.5834 & -0.7084 & -1.2916 \\ 0.5834 & 1.4166 & -1.2916 & -0.7084 \\ -0.7084 & -1.2916 & 1.4166 & 0.5834 \\ -1.2916 & -0.7084 & 0.5834 & 1.4166 \end{bmatrix} + \begin{bmatrix} 1.4166 & 0.5834 & -0.7084 & -1.2916 \\ 0.5834 & 1.4166 & -1.2916 & -0.7084 \\ -0.7084 & -1.2916 & 1.4166 & 0.5834 \\ -1.2916 & -0.7084 & 0.5834 & 1.4166 \end{bmatrix} \right] \tag{29}$$

The assembled $K_{ij}{}^{e}$ matrix using Figure 2 becomes Equations (30) and (31)

$$K_{ij}{}^{e} = \begin{bmatrix} K_{11}^1 & K_{12}^1 & 0 & K_{14}^1 & K_{13}^1 & 0 & 0 & 0 & 0 \\ K_{21}^1 & K_{22}^1 + K_{11}^2 & K_{12}^2 & K_{24}^1 & K_{23}^1 + K_{14}^2 & K_{23}^2 & 0 & 0 & 0 \\ 0 & K_{21}^2 & K_{22}^2 & 0 & K_{24}^2 & K_{23}^2 & 0 & 0 & 0 \\ K_{41}^1 & K_{42}^2 & 0 & K_{44}^1 + K_{11}^3 & K_{43}^1 + K_{12}^3 & 0 & K_{14}^3 & K_{13}^3 & 0 \\ K_{31}^1 & K_{32}^1 + K_{41}^2 & K_{42}^2 & K_{34}^1 + K_{21}^3 & K_{33}^1 + K_{44}^2 + K_{22}^3 + K_{11}^4 & K_{43}^2 + K_{12}^4 & K_{24}^3 & K_{23}^3 + K_{14}^4 & K_{13}^4 \\ 0 & K_{31}^2 & K_{32}^2 & 0 & K_{34}^2 + K_{21}^4 & K_{33}^2 + K_{22}^4 & 0 & K_{24}^4 & K_{23}^4 \\ 0 & 0 & 0 & K_{41}^3 & K_{42}^4 & 0 & K_{44}^4 & K_{43}^4 & 0 \\ 0 & 0 & 0 & K_{31}^3 & K_{32}^3 + K_{41}^4 & K_{42}^4 & K_{34}^3 & K_{33}^3 + K_{44}^4 & K_{43}^4 \\ 0 & 0 & 0 & 0 & K_{31}^4 & K_{32}^4 & 0 & K_{34}^4 & K_{33}^4 \end{bmatrix} \tag{30}$$

$$K_{ij}{}^{e} = \begin{bmatrix} 1.4166 & 0.5834 & 0 & -1.2916 & -0.7084 & 0 & 0 & 0 & 0 \\ 0.5834 & 2.8332 & 0.5834 & -0.7084 & -2.5832 & -1.2916 & 0 & 0 & 0 \\ 0 & 0.5834 & 1.4166 & 0 & -0.7084 & -1.2916 & 0 & 0 & 0 \\ -1.2916 & -0.7084 & 0 & 2.8331 & 1.1668 & 0 & -1.2916 & -0.7084 & 0 \\ -0.7084 & -2.5832 & -0.7084 & 2 & 5.6664 & 1.1668 & -0.7084 & -2.5832 & -0.7084 \\ 0 & -0.7084 & -1.2916 & 0 & 1.1668 & 1.1668 & 0 & -0.7084 & -1.2916 \\ 0 & 0 & 0 & -0.7084 & -1.2916 & 0 & 0.5834 & 1.4166 & 0 \\ 0 & 0 & 0 & -0.7084 & -2.5832 & -0.7084 & 0.5834 & 2.8332 & 0.5834 \\ 0 & 0 & 0 & 0 & -0.7084 & -1.2916 & 0 & 0.5834 & 1.4166 \end{bmatrix} \tag{31}$$

Applying the boundary conditions on Equations (4) through (7), yielded Equation (32).

$$\{Q_{ij}{}^{e}\} = \begin{Bmatrix} 0 \\ 0 \\ 0 \\ 0 \\ 1 \\ 0 \\ 0 \\ 1 \\ 0 \end{Bmatrix} \tag{32}$$

We substituted Equations (31) and (32) into Equation (13) and obtained Equation (33)

$$\begin{bmatrix} 1.4166 & 0.5834 & 0 & -1.2916 & -0.7084 & 0 & 0 & 0 & 0 \\ 0.5834 & 2.8332 & 0.5834 & -0.7084 & -2.5832 & -1.2916 & 0 & 0 & 0 \\ 0 & 0.5834 & 1.4166 & 0 & -0.7084 & -1.2916 & 0 & 0 & 0 \\ -1.2916 & -0.7084 & 0 & 2.8331 & 1.1668 & 0 & -1.2916 & -0.7084 & 0 \\ -0.7084 & -2.5832 & -0.7084 & 2 & 5.6664 & 1.1668 & -0.7084 & -2.5832 & -0.7084 \\ 0 & -0.7084 & -1.2916 & 0 & 1.1668 & 1.1668 & 0 & -0.7084 & -1.2916 \\ 0 & 0 & 0 & -0.7084 & -1.2916 & 0 & 0.5834 & 1.4166 & 0 \\ 0 & 0 & 0 & -0.7084 & -2.5832 & -0.7084 & 0.5834 & 2.8332 & 0.5834 \\ 0 & 0 & 0 & 0 & -0.7084 & -1.2916 & 0 & 0.5834 & 1.4166 \end{bmatrix} \begin{Bmatrix} u_1 \\ u_2 \\ u_3 \\ u_4 \\ u_5 \\ u_6 \\ u_7 \\ u_8 \\ u_9 \end{Bmatrix} = \begin{Bmatrix} 0 \\ 0 \\ 0 \\ 0 \\ 1 \\ 0 \\ 0 \\ 1 \\ 0 \end{Bmatrix} \quad (33)$$

3. Results and Discussion

"Table 1" shows the results for the finite element analysis. Figure 3, are the graphs of velocity against nodal values, showing the velocity profile at different cross sections along the mould's sprue. These profiles are parabolic in shape with the maximum velocity at the center.

Table 1. Finite Element Results

Nodes	U	Velocity (mm/s)
1	u_1	1.1152
2	u_2	1.1108
3	u_3	0.000
4	u_4	1.0088
5	u_5	1.3055
6	u_6	0.000
7	u_7	0.7337
8	u_8	1.7030
9	u_9	0.000

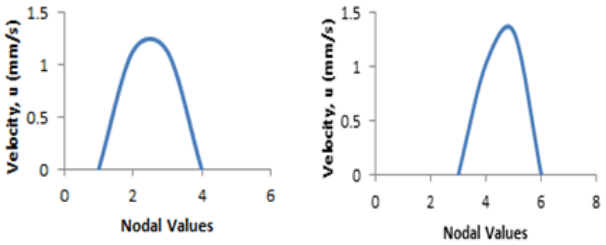

Figures 3(a) and (b). Graphs of velocity against nodal values showing the velocity profile at different cross sections along the mould's sprue in gravity sand casting

The maximum velocity of molten metal flow obtained from this work (2565mm/s), when compared with the work of Rohaya [19] (Table 2 and Figure 4) which ranged from 2300mm/s to 3200mm/s showed that the danger of casting defects as a result of molten metal flow above the critical velocity can be avoided. Meanwhile below the critical velocity the melt was safe from entrainment problem.

The solutions obtained from this work (2565mm/s) were also compared with the work of Feng [1] (Table 3 and Figure 5) which ranged from 260mm/s to 2850mm/s, the comparison showed that the danger of air entrainment leading to defect as a result of molten metal flow above the critical velocity can be avoided.

Table 2. Comparison between this work and Rohaya [19]

Z	This Work	Rohaya
1	135.76	500
2	2245.54	2300
3	2564.81	3200
4	0.0000	0.000

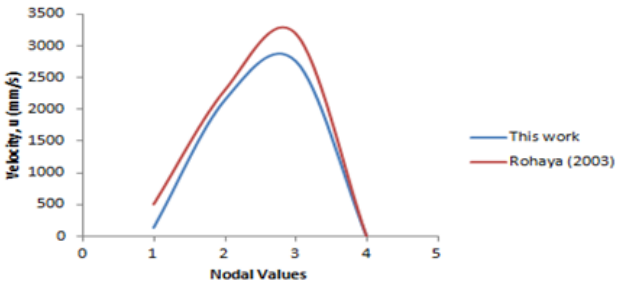

Figure 4. Graph of velocity against nodal values showing the velocity profile at a cross section along the sprue in gravity sand casting for this work and Rohaya.

Table 3. Comparison between this work and Feng [1].

Z	This Work	Feng
1	135.76	260
2	2245.54	2450
3	2564.81	2850
4	0.0000	0.000

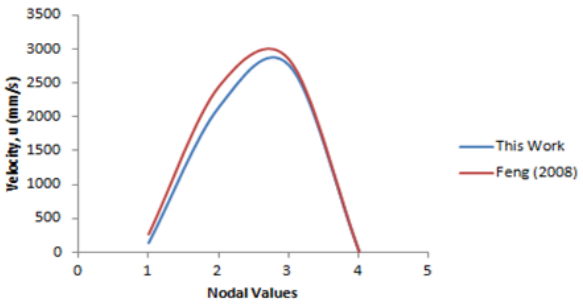

Figure 5. Graph of velocity against nodal values showing the velocity profile at a cross section along the sprue in gravity sand casting for this work and Feng [1]

The maximum velocity of molten metal flow obtained from this work (2565mm/s), when compared with the work of Inegbedion and Akpobi [20] (Table 4 and Figure

6) which ranged from 130.76mm/s to 2754.81mm/s showed that the danger of casting defects as a result of molten metal flow above the critical velocity can be avoided. Meanwhile below the critical velocity the melt was safe from entrainment problem.

Table 4. Comparison between this work and Inegbedion and Akpobi [20]

Z	This Work	Inegbedion and Akpobi
1	135.76	130.76
2	2245.54	2135.54
3	2564.81	2754.81
4	0.0000	0.0000

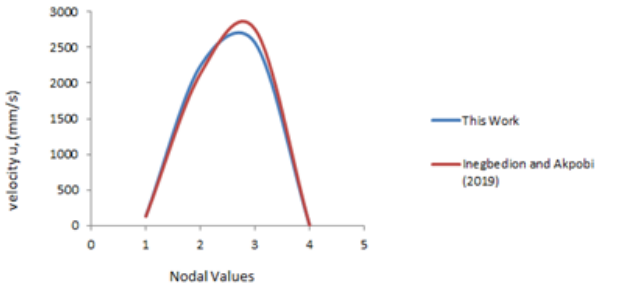

Figure 6. Graph of velocity against nodal values showing the velocity profile at a cross section along the sprue in gravity sand casting for this work and Inegbedion and Akpobi [20]

To validate the results obtained, we produced various casts using these results. The cast produced showed that sprue height below the critical drop height prevented casting defects associated with pouring velocities while sprue height above the critical drop height the danger of casting defects associated with pouring velocities above the critical velocity could not be avoided.

"Figure 7", showed the various surface defects that can occur in casting when cast are produced using sprue height above the critical drop height (377mm): The molten metal is not safe from casting defects because the pouring velocity exceeded the critical flow velocity. These defects can be avoided with pouring velocities below the critical velocity (Figure 8).

It is evident from Figure 8 that all casting defects associated with pouring, using sprue height above the critical drop height, can be avoided if cast can be produced using sprue heights below the critical drop height. In this case, the melt is safe since the pouring velocity is below the critical velocity.

4. Conclusion

Results obtained from the analysis of molten metal flow showed that there exist a critical velocity and critical drop height for molten metal flow, to prevent entrainment of air and porosity problem in casting.

The finite element analysis of molten metal flow in the mould sprue using continuity equation was used in this research work. The velocity distribution of the flow of molten metal were developed using the finite element method. The weighted integral of the equation was obtained, the weak form of the equation was developed and the finite element model was determined. The various matrices were assembled, solved and solutions obtained by using an eight linear element of nine nodes and a four linear rectangular element. By using appropriate interpolation function and boundary conditions, the solutions to the equations were obtain and validated using relevant literatures.

(A) (B)

Figure 7. Cast produced for different sprue height above the critical drop height: (a) 450mm sprue height (b) 400mm sprue height. The critical drop height is 377mm.

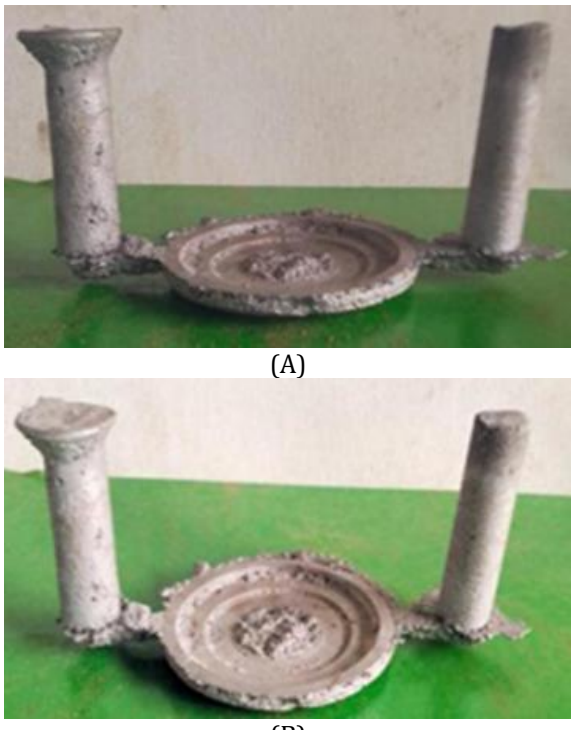

(A)

(B)

Figure 8. cast produced for different sprue height below the critical drop height: (a) 250mm sprue height (b) 220mm sprue height. The critical drop height is 377mm

Finally, to avoid entrainment of air and porosity problems in casting, the critical velocity and critical drop

height of molten metal as it flows down the sprue of casting mould was established. Further analysis of the flow of fluid in casting mould showed that molten metal flow below the critical velocity will prevent casting defects because flow is smooth and laminar. The critical drop height obtained from this work was used to produce various casts. The results obtained showed that casting defects can be avoided when cast are produced using sprue height below the critical drop height while cast produced using sprue height above the critical drop height the danger of casting defects could not be avoided. Therefore, the critical velocity and critical drop height obtained in this work will prevent air entrainment and porosity problem in casting. Consequently, foundry engineers will no longer rely on their individual knowledge and experience or perform trial and error runs before carrying out any casting process. This will reduce casting development cycle, defects and production time.

Author contributions

Francis Inegbedion: Conceptualization, Visualization, Methodology, Investigation, Writing-Reviewing and Editing **James Chinedu Orji:** Methodology, Investigation, Data curation, Writing-Original draft preparation

Conflicts of interest

The authors declare no conflicts of interest.

References

1. Feng L., (2008). Optimized Design of Gating/Riser System in Casting Based on CAD and Simulation Technology, Submitted to the faculty of the Worchester Polytechnic Institute in partial fulfillment of the requirements for degree of Master of science in Manufacturing Engineering.
2. Attar E.H., Babaei R.P., Asgari K., Davami P., (2005). Modelling of air pressure effects in casting moulds, Journal of Modelling and Simulation in Materials Science and Engineering, 13, 903-917
3. Lee P. D., Chirazi A., & See D. (2001). Modelling micro porosity in Aluminium - Silicon alloys: a review, Journal of Light Metals, 1, 15-30
4. Sowa L. (1998). Model of the Casting Solidification taking into consideration the motion of liquid phase, Archives of Mechanical technology and Automatization, 18, 287 – 296
5. Sowa, L., (2010). Mathematical Modelling of the Filling Process of a slender mould cavity, Scientific Research of the Institute of Mathematics and Computer Science, 9(2) 219-227
6. Salih A. (2011). Conservation Equations of fluid Dynamics, Department of Aerospace Engineering, Indian Institute of space Science and technology, Thiruvananthapuram publishers 4-7
7. Sowa L. & Bokota A. (2007). Numerical Modelling of Thermal and Fluid Flow Phenomena in the Mould Channel, Archives of Foundry Engineering, 7(4), 165 – 168.
8. Sowa, L., (2010), Numerical Analysis of the Thermal and Fluid Flow Phenomena of the Fluidity test, Archives of Foundry Engineering, 10(1), 157 – 160.
9. Bird R. B., Stewart W.E., & Lightfoot E.N., (2002). Transport Phenomena, 2nd edition, Wiley: NY.
10. Aris, R., (1962). Vectors, Tensors, and the Basic Equations o Fluid Mechanics, Prentice Hall Publishers, Englewood Cliffs, NJ
11. Ik-Tae I., Woo-Seung K., & Kwan-Soo L., (2001). A unified analysis of filling and solidification in casting with natural convection, International Journal of Heat and Mass Transfer, 44, 1507-1515
12. Sowa, L., Sczygiol, N. Domoilski, T., & Bokota, A., (2008). Simplified Model of Metal Solidification in the Thin Plane Cavity of the Casting Mould, Archives of Foundry Engineering, 8(1), 309 – 312
13. Bokota A. & Sowa L. (2010). Numerical Modelling of the thermal and fluid flow phenomena of the fluidity test, Archives of Foundry Engineering 10(1), 15–18
14. Mishima S., & Szekely J. (1989). The modelling of fluid flow and heat transfer in mould filling, ISIJ International, 29(4), 324-332
15. Majchrzak E., Jasinski M., & Kaluza G. (2004). Sensitivity analysis of solidification process with respect to the geometrical parameters of casting and mould, Archives of Foundry Engineering, 4(14) 279-284.
16. Reddy J. N., (2006). An Introduction to the Finite Element Method, Third Edition, International Edition McGraw- Hill., 146 – 147, 441 - 442.
17. Singiresu S. R. (2004). The Finite Element Methods in Engineering, fourth edition, Elsevier Science and Technology Books Publisher
18. Hutton V. D. (2004). Fundaments of Finite Element Analysis, 1st Edition, McGraw-Hill Companies, Inc. 293 – 295
19. Rohaya B. D. (2013). Design and Analysis of Casted LM6 - TIC in Designing of Production Tooling, Faculty of Manufacturing Engineering, Universiti Teknikal Malaysia Melaka (UTEM) 63 – 69
20. Inegbedion F. and Akpobi J.A. (2019). Determination of the Critical Velocity of Molten Metal Flow in Casting Mould Sprue, International Journal of Engineering Trends and Technology (IJETT) – 67(10), 27 – 33.